A&A 366, 898–912 (2001)
DOI: 10.1051/0004-6361:20000269

Astronomy & Astrophysics

The stellar content of the Hamburg/ESO survey*

I. Automated selection of DA white dwarfs

N. Christlieb[1], L. Wisotzki[2], D. Reimers[1], D. Homeier[3], D. Koester[3], and U. Heber[4]

[1] Hamburger Sternwarte, Universität Hamburg, Gojenbergsweg 112, 21029 Hamburg, Germany
e-mail: nchristlieb/dreimers@hs.uni-hamburg.de
[2] Institut für Physik, Universität Potsdam, Am Neuen Palais 10, 14469 Potsdam, Germany
e-mail: lutz@astro.physik.uni-potsdam.de
[3] Institut für Theoretische Physik und Astrophysik der Christian-Albrechts-Universität Kiel, Leibnizstrasse 15, 24098 Kiel, Germany
e-mail: homeier/koester@astrophysik.uni-kiel.de
[4] Dr. Remeis Sternwarte, Universität Erlangen-Nürnberg, Sternwartstrasse 7, 96049 Bamberg, Germany
e-mail: heber@sternwarte.uni-erlangen.de

Received 30 August 2000 / Accepted 14 November 2000

Abstract. We describe automatic procedures for the selection of DA white dwarfs in the Hamburg/ESO objective-prism survey (HES). For this purpose, and the selection of other stellar objects (e.g., metal-poor stars and carbon stars), a flexible, robust algorithm for detection of stellar absorption and emission lines in the digital spectra of the HES was developed. Broad band ($U-B$, $B-V$) and intermediate band (Strömgren c_1) colours can be derived directly from HES spectra, with precisions of $\sigma_{U-B} = 0.092$ mag; $\sigma_{B-V} = 0.095$ mag; $\sigma_{c_1} = 0.15$ mag. We describe simulation techniques that allow one to convert model or slit spectra to HES spectra. These simulated objective-prism spectra are used to determine quantitative selection criteria, and for the study of selection functions. We present an atlas of simulated HES spectra of DA and DB white dwarfs. Our current selection algorithm is tuned to yield maximum efficiency of the candidate sample (minimum contamination with non-DAs). DA candidates are selected in the $B-V$ versus $U-B$ and c_1 versus $W_\lambda(\mathrm{H}\beta+\mathrm{H}\gamma+\mathrm{H}\delta)$ parameter spaces. The contamination of the resulting sample with hot subdwarfs is expected to be as low as ∼8%, while there is essentially no contamination with main sequence or horizontal branch stars. We estimate that with the present set of criteria, ∼80% of DAs present in the HES database are recovered. A yet higher degree of internal completeness could be reached at the expense of higher contamination. However, the external completeness is limited by additional losses caused by proper motion effects and the epoch differences between direct and spectral plates used in the HES.

Key words. surveys – methods: data analysis – white dwarfs

1. Introduction

The Hamburg/ESO survey (HES) is an objective prism survey primarily targeting bright quasars (Wisotzki et al. 1996; Reimers & Wisotzki 1997; Wisotzki et al. 2000). However, because its spectral resolution is typically 15 Å FWHM at Hγ, it is also possible to efficiently select a variety of interesting *stellar* objects in the HES. These include, e.g., metal-poor halo stars, carbon stars, cataclysmic variable stars, white dwarfs (WDs), subdwarf B stars (sdBs), subdwarf O stars (sdOs), and field horizontal branch A- and B-type stars (Christlieb 2000). In a series of papers, we will report on the development of quantitative selection procedures for the systematic exploitation of the stellar content of the HES, and their application to the digital HES data base. In this paper, we report on an automatic algorithm for the selection of DA white dwarfs (DAs).

The aim of the DA selection in the HES described in this paper is to test the double-degenerate (DD) scenario for SN Ia progenitors, in which a binary consisting of two WDs of large enough mass, merges and produces a thermonuclear explosion. If this scenario is correct, SN Ia progenitor systems should be present among DDs, the latter being identifiable by radial velocity (RV) variations. Although several double degenerates have been found, none of them is sufficiently massive to qualify as a viable

Send offprint requests to: N. Christlieb
* Based on observations collected at the European Southern Observatory, La Silla and Paranal, Chile.

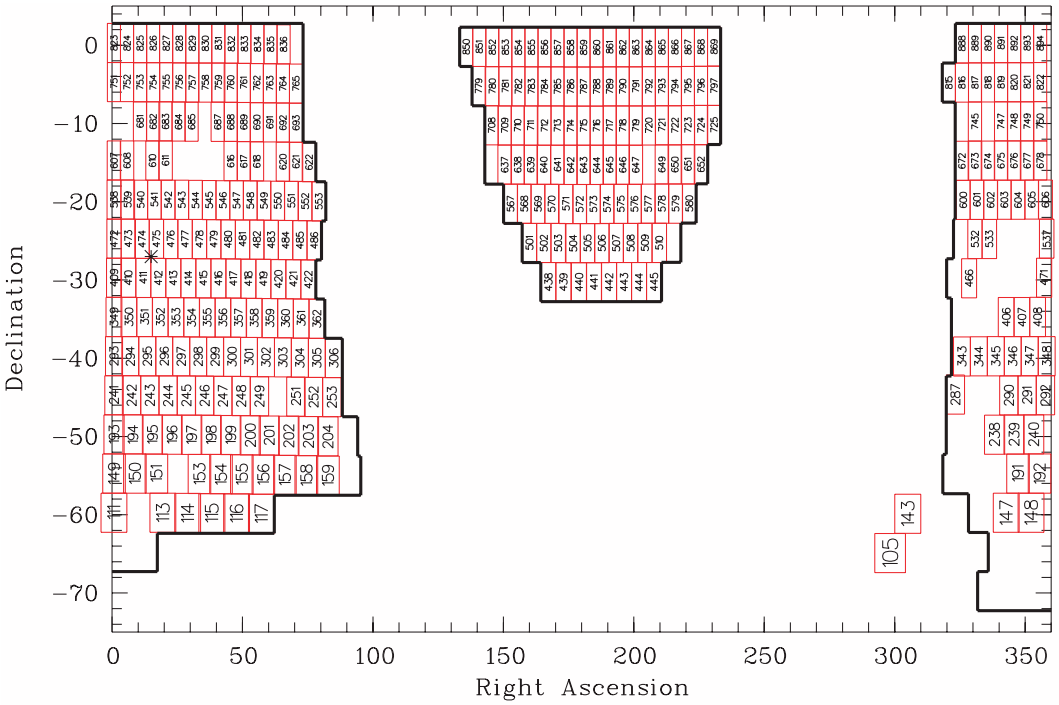

Fig. 1. Definition of HES area (framed) and numbers of fields in which the exploitation of the stellar content of the HES is currently carried out. For orientation, the position of the southern galactic pole is marked with "∗" (lower left corner of field 475)

SN Ia progenitor (see Maxted & Marsh 1999). Note however that recently a system consisting of a sdB and a massive white dwarf has been found, the total mass of which exceeds the Chandrasekhar mass (Maxted et al. 2000). In order to increase the sample of DDs, a *Large Programme* was proposed to (and accepted by) the European Southern Observatory (ESO), aiming at observing a large (∼1 500) sample of WDs with VLT Unit Telescope 2 (UT2), and its high resolution spectrograph UVES, at randomly chosen epochs, dictated by observing conditions. That is, every time the weather is *too bad* to carry out Service Mode observations for other programs, WDs are observed.

A program like this requires a large catalog of targets spread all over the accessible sky in order to be successful. From the "Catalog of Spectroscopically Identified White Dwarfs" of McCook & Sion (1999) it is evident that the southern sky has not yet been surveyed as extensively for white dwarfs as the northern sky: only 33% of the objects listed are located at $\delta < 0°$. Therefore, we were aiming at selecting additional targets in the data base of the HES.

White dwarfs have been selected from wide angle surveys in the southern hemisphere before, and also in the HES (see below). "Classical" UV excess surveys, like the Montreal-Cambridge-Tololo survey (MCT; Demers et al. 1986; Lamontagne et al. 2000), or the Edinburgh-Cape survey (EC; Stobie et al. 1997; Kilkenny et al. 1997) can efficiently select complete samples of hot stars, including WDs. However, completeness at the *cool* end is either sacrificed for efficiency, as in the MCT (see Fig. 2), where only objects with $U - B < -0.6$ enter the sample of stars for which follow-up spectroscopy is obtained (Lamontagne et al. 2000), or efficiency is sacrificed for completeness, as in the EC. It has been shown that the EC is 94% complete for objects of $U - B < -0.4$ down to $B = 16.5$ (Stobie et al. 1997). However, an intermediate selection step based on photoelectric UBV photometry has to be used to eliminate the large fraction (∼30%; see Kilkenny et al. 1997) of "normal" F and G type stars.

In the HES, WDs enter the quasar candidate sample if they have $U - B < -0.18$ (Wisotzki et al. 2000). However, HES quasar candidates are inspected manually at the computer screen, and in this process hot stars, and stars clearly exhibiting stellar absorption lines (like e.g. DA white dwarfs, having strong, broad lines over a wide temperature range; see Fig. B.1 in Appendix B) are rejected, and follow-up spectroscopy is not obtained for them in the course of the quasar survey. This results in a very efficient quasar selection: typically 70% of the objects for which follow-up spectroscopy is obtained *are* quasars (Wisotzki et al. 2000). The remaining 30% are mainly hot subdwarfs, and cool ($T_{\rm eff} \lesssim 20\,000\,{\rm K}$), helium-rich WDs (DBs, DZs; see Friedrich et al. 2000). A couple of interesting peculiar objects, e.g., magnetic DBs (Reimers et al. 1998) and magnetic DAs (Reimers et al. 1994, 1996) have also been discovered in this way.

The selection of white dwarf candidates described in this paper aims at an *efficient* selection; that is, the contamination of the sample with other objects (e.g., hot subdwarfs) shall be as clean as possible, in order not to waste any observing time at the VLT.

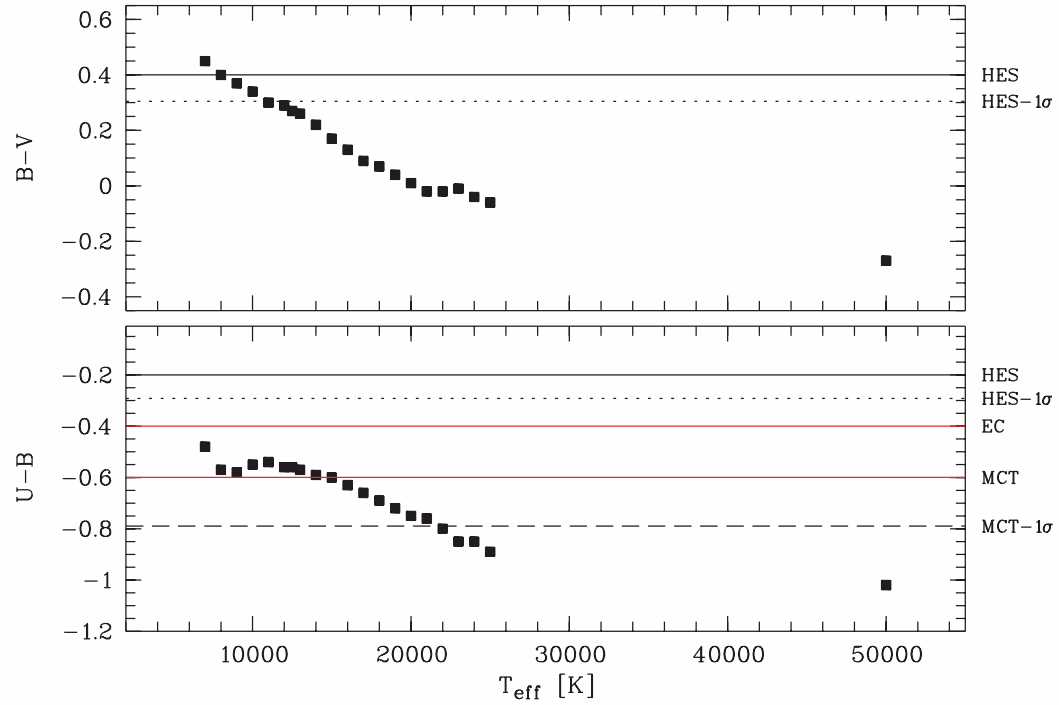

Fig. 2. $U-B$ and $B-V$ for DAs as a function of effective temperature, determined with model spectra. Taking into account the rms error in $U-B$ of 0.18 mag in the MCT survey, the adopted selection criterion of $U-B<-0.6$ leads to rejection of cool ($T_{\rm eff}\lesssim 22\,000$ K) DA white dwarfs. In the HES, only DAs of $T_{\rm eff}\lesssim 11\,000$ K are expected to be lost when the selection criteria described in Sect. 5 are applied

2. The HES data base

A description of the HES plate material, plate digitisation and data reduction can be found in Wisotzki et al. (2000). In this section we describe some survey properties that are particularly important for stellar work in more detail than it was done in Wisotzki et al. (2000), and we briefly repeat a general description of the HES, for better readability.

The HES is based on IIIa-J plates taken with the 1 m ESO Schmidt telescope and its 4° prism. It covers the magnitude range $13.0\gtrsim B_{\rm J}\gtrsim 17.5$ (Wisotzki et al. 2000). The magnitude limits depend on plate quality. Note that the value given for the faint limit is the completeness limit for quasar search, which we define as the magnitude corresponding to average photographic density in the $B_{\rm J}$ band $>5\sigma$ above the diffuse plate background, where σ is the background noise. The detection limit of the HES is approximately one magnitude deeper than the completeness limit. For stellar applications, the survey magnitude range depends on the object type searched for. E.g., in our search for metal-poor stars, we only use spectra that are not affected by saturation effects, which typically start to be noticable at $B_{\rm J}\sim 14.0$, and we only include spectra with $S/N>10$ (which roughly corresponds to $B_{\rm J}\sim 16.4$), because at lower S/N an efficient selection of metal-poor stars, by means of a weak or absent Ca K line, is not feasible anymore. However, for most other object types, including DAs, we adopt the 5σ magnitude limit.

The atmospheric cutoff at the blue end, and the sharp sensitivity cutoff of the IIIa-J emulsion ("red edge") result in a wavelength range of 3200 Å $<\lambda<$ 5300 Å (see Fig. 3). The spectral resolution of the HES is primarily seeing-limited. For plates taken during good seeing conditions, the pixel spacings chosen in the digitization process result in an under-sampling, so that in these cases the spectral resolution is also limited by the sampling.

The definition of the HES survey area makes use of the mean star density and average column density of neutral hydrogen for each ESO/SERC field (Wisotzki et al. 2000). The adopted criteria roughly correspond to galactic latitudes of $|b|>30°$. The declination range covered by the HES is $+2.5°>\delta>-78°$. As a result, the survey area consists of 380 fields. Between 1989 and 1998, objective-prism plates were taken for all of these, and the plates were subsequently digitized and reduced at Hamburger Sternwarte. As one ESO Schmidt plate covers approximately $5\times 5\,{\rm deg}^2$ on the sky, the nominal survey area is $9\,500\,{\rm deg}^2$, or the total southern extragalactic sky. Note, however, that the *effective* survey area is ∼25% lower, mainly because of overlapping spectra (Wisotzki et al. 2000).

2.1. Detection of overlapping spectra

Overlapping spectra (hereafter shortly called overlaps) are detected automatically using the direct plate data of the Digitized Sky Survey I (DSS I). For each spectrum to be

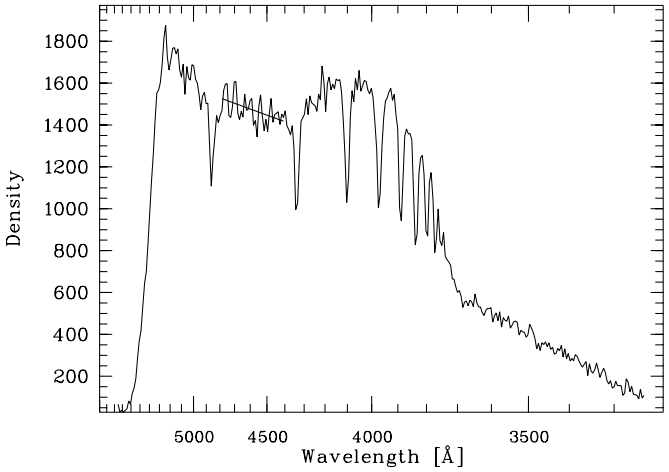

Fig. 3. Measurement of noise in an absorption line free spectral region of A-type stars. Note that we plot HES objective prism spectra such that wavelengths are *decreasing* towards the right, because the scan length x is *increasing* in this direction. The sharp drop of the spectra at the red end is due to the IIIa-J emulsion sensitivity cutoff at ∼5400 Å

extracted, it is looked for objects in the dispersion direction on the direct plate. If there is one, the automatic procedure marks the corresponding spectrum, so that it can later be excluded from further processing, if this is desired. *It is* desired for stellar work, since the feature detection and object selection algorithms would get confused otherwise, and a lot of "garbage" would enter the candidate samples. The digital HES data base for stellar work consists of ∼4 million extracted, overlap-free spectra with average $S/N > 5$ in the $B_{\rm J}$ band.

2.2. Photometry

As described in Wisotzki et al. (2000), the calibration of HES $B_{\rm J}$ magnitudes is done plate by plate with individual photometric sequences. The $B_{\rm J}$ band is formally defined by the spectral sensitivity curve of the Kodak IIIa-J emulsion multiplied with the filter curve of a Schott GG395 filter. The overall errors of the HES $B_{\rm J}$ magnitudes, including zero point errors, are less than ±0.2 mag. Note that $B_{\rm J}$ can be converted to B using the formula

$$B = B_{\rm J} + 0.28 \cdot (B - V), \tag{1}$$

which is valid for main sequence stars in the colour range $-0.1 < (B - V) < 1.6$ (Hewett et al. 1995).

2.3. Wavelength calibration

A global dispersion relation for all HES plates was determined by using A-type stars. In HES spectra of these stars the Balmer lines at least up to H_{10} are resolved (see Fig. 3), so that a dispersion relation can be derived by comparing the x-positions (scan length in μm) of these lines with the known wavelengths. Borra et al. (1987) used the position of the "red edge" of objective-prism spectra to determine the zero point of the wavelength calibration, but noticed that the position depends on the energy distribution of the object. Therefore, in the HES we decided to use a zero point specified by an astrometric transformation between direct plates and spectral plates. The wavelength calibration is accurate to ±10 μm. This corresponds to ±4.5 Å at Hγ and ±2.3 Å at $\lambda = 3500$ Å.

2.4. Estimation of the amplitude of pixel-wise noise

Following the approach of Hewett et al. (1985), we determine the amplitude of pixel-wise noise as a function of photographic density D plate by plate using A- and F-type stars. A straight line fit is done to the spectral region between Hβ and Hγ (see Fig. 3). The 1 σ-scatter around this pseudo-continuum fit is taken as noise amplitude. In this approach we assume that the scatter is mainly due to noise, since in early-type stars the spectral region under consideration includes only very few absorption lines at the spectral resolution of the HES. Moreover, it is expected that the population of A- and F-type stars found at high galactic latitudes is dominated by metal-poor stars, so that metal lines are usually very weak. However, we cannot exclude that we overestimate the noise by a few percent due to contributions of metal lines to the scatter around the pseudo-continuum fit.

We measure the noise amplitude for all A- and F-type stars present on each HES plate (typically several hundred per plate), and compute the mean density D in the fit region. This yields data points (D, noise), to which a 2nd order polynomial is fitted, i.e.

$$\text{noise} = a_0 + a_1 \cdot D + a_2 \cdot D^2. \tag{2}$$

Note that in the HES, D refers to density above diffuse plate background (bgr) in arbitrary units called counts. The relation between counts and photographic densities $D_{\rm photo}$ is

$$D_{\rm photo} = \frac{D\,[\text{counts}] + D_{\rm bgr}\,[\text{counts}]}{800}. \tag{3}$$

For the determination of the coefficients $a_0 \ldots a_2$ we use a robust fit algorithm which minimizes the sum of absolute deviations, taking into account the following set of boundary conditions:

- $a_0 > 0$. The noise at $D = 0$ is the noise of the plate background, which is always > 0;
- $a_2 \geq 0$. Since $D \geq 0$, and the noise increases monotonically with D, a_2 must be positive (or zero);
- $a_1 \geq 0$. From the previous boundary condition follows that the polynomial has a minimum at $D_{\rm min} = -a_1/(2a_2)$. Using again the argument that the noise increases monotonically with D, it follows that $D_{\rm min} \leq 0$. Since $a_2 \geq 0$, a_1 must be ≥ 0.

An example for a such a fit is shown in Fig. 4.

For simulations of spectra (see Sect. 4) it is very important to know the *form* of the distribution of noise.

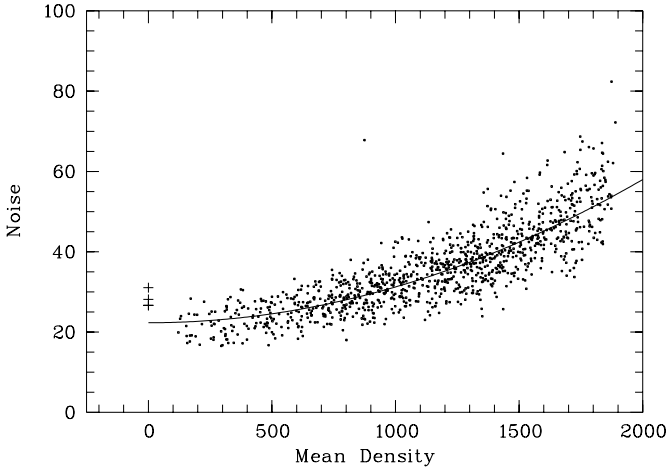

Fig. 4. Fitting of a 2nd order polynomial to data points (D, noise), for estimation of pixel-wise noise as a function of density. The plate background noise of each plate quarter is marked with "+". It is always higher than expected from the noise parabola fit, since the optimal spectrum extraction algorithms result in a bias towards lower noise

We investigated this by using 50 spectra of A-type stars from eight plates with high sky background ($D_{\mathrm{bgr}} > 1\,500$), and 60 spectra from seven plates with low background ($D_{\mathrm{bgr}} < 700$). These spectra were chosen by hand from the sample of automatically selected A-type stars, in order to ensure that misclassified spectra, and spectra for which the fit of the continuum between Hβ and Hγ by a straight line is not fully adequate, do not confuse the results. Five of the original set of 115 spectra were excluded in the manual selection process.

The deviations from the continuum fits were collected for each spectrum, shifted to a median of zero, and divided by the average of the absolute values of the upper and lower 50% quartile, so that a comparison of the noise distributions measured in different spectra (with different noise amplitude) is possible. The result is that the distribution of pixel-wise noise is almost perfectly Gaussian, independently of plate background (see Fig. 5).

Figure 6 shows the relation between average pixel-wise S/N in the B_{J} band and B_{J} magnitudes for 589 not saturated point sources from many different HES plates. The large scatter of S/N for given B_{J} shown in this plot is due to varying plate background, and seeing.

3. Feature detection

3.1. Detection of stellar lines

It is critical for all quantitative selection methods to have a set of *reliable* features at hand. The total set of available features should contain as much information of the objects to be classified as possible. Therefore, we implemented a flexible, robust algorithm which allows to detect stellar absorption and/or emission lines in HES spectra. Hewett et al. (1985) used a template matching technique to automatically detect absorption and emission lines in objective-prism spectra. Tests with HES spectra have shown that a fit algorithm involving a couple of boundary conditions (see below) is much more stable and leads to more accurate measurements of equivalent widths than template matching. The algorithm used in the HES consists of the following steps:

1. Determination of continuum by filtering with a wide median filter and narrow Gaussian filter. A similar filtering technique was also used by Hewett et al. (1985) and Borra et al. (1987).
2. Improvement of determination of the wavelength calibration zero point by fitting of three sets of stellar lines. The sets contain the strongest stellar absorption lines of early type, solar type, and late type stars, respectively. The individual line depths, and the zero point offset of wavelength calibration are fitted simultaneously. The *relative* positions of the stellar lines are held fixed, and the line *width* is held fixed at the value of the seeing profile width, which is measured during spectral extraction. The set of lines giving the strongest signal, i.e. largest average equivalent widths, is selected, and the wavelength calibration zero point determined with that fit is adopted.
3. Improvement of continuum determination:
   a. Fitting of *all* stellar lines detectable in HES spectra.
   b. Subtraction of fitted lines from the original spectrum.
   c. Computation of improved continuum by filtering the line-subtracted spectrum again with a wide median filter and narrow Gaussian filter.
   d. Go back to 3a, if $n_{\mathrm{iter}} < 3$; otherwise compute rectified spectrum with final continuum.
4. Fitting of all stellar lines in the rectified spectrum by Gaussians.

For each spectral line it can be chosen whether it is to be detected in absorption or emission. The output of the fit algorithm are equivalent width, FWHM and S/N of the lines, and shift of the wavelength calibration zero point. Any spectral lines not yet considered can easily be included by just adding its wavelength to the list of lines to be fitted. In this work we make use of the equivalent widths of Hβ, Hγ and Hδ only, which are summed to the parameter `balmsum`.

3.2. Broad band and intermediate band colours

As already noticed by Hewett et al. (1985), relative colours can be determined quite accurately directly from objective-prism spectra. Hewett et al. (1995) used so-called "half power points (hpps)" to measure relative colours, that is, bisecting points of the photographic density distribution. hpps are equivalent to broad-band colours, but have the advantage of being more robust against noise. Wisotzki et al. (2000) introduced half power

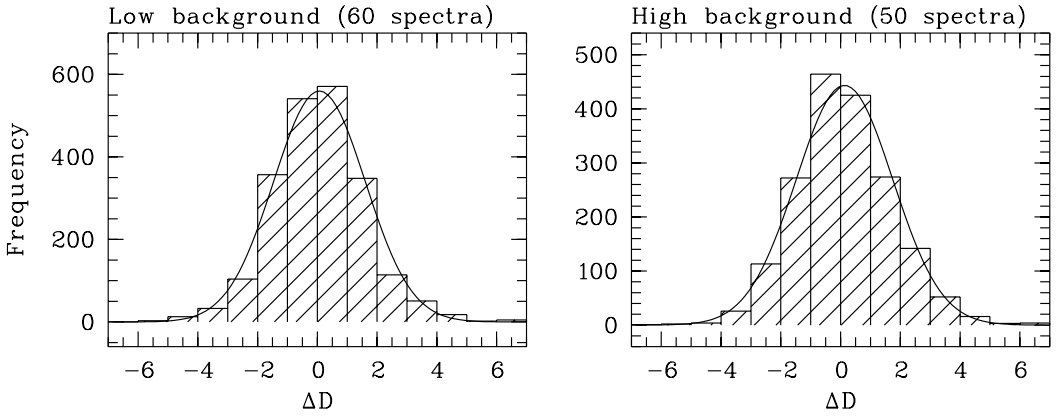

Fig. 5. Distribution of pixel-wise noise in absorption line free regions of 60 spectra of A-type stars from seven plates with low sky background (left panel), and 50 spectra from eight plates with high background (right panel). For further explanation see text

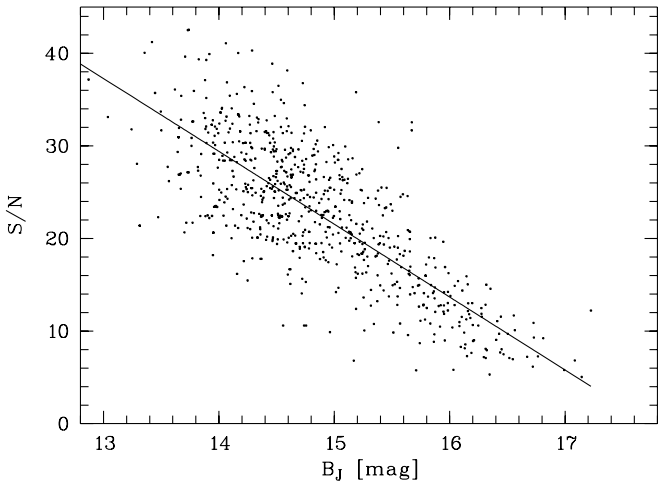

Fig. 6. Average pixel-wise S/N in the B_J band as a function of B_J for 589 not saturated point sources from more than 100 different HES plates. The straight line fit corresponds to $B_J = 17.7 - 0.13 \cdot S/N$

points that are computed only for a *part* of the spectrum (see Fig. 7). The half power points `x_hpp1` and `x_hpp2` are well correlated with $U-B$ and $B-V$, respectively.

Since it is helpful in many stellar applications to have not only relative, but calibrated $U-B$ and $B-V$ colours at hand, we established calibrations of `x_hpp1` and `x_hpp2` versus $U-B$ and $B-V$, respectively.

A more precise colour calibration can be achieved when distances `dx` to a cutoff line in a colour-magnitude diagram (see Fig. 8) is used instead of `x` values (scan length in μm) for the bisecting point, because plate-to-plate variations of the spectral sensitivity curves are compensated in this way. The cutoff line separates the bulk of "normal" stars from UV-excess objects (or objects with unusually low $B-V$ in case of `dx_hpp2`). The cutoff is determined by a break finding algorithm.

Because the blue end of the HES spectra is sensitive to contamination by overlaps, special care must be taken to exclude such spectra from the calibration of `dx_hpp1`. This was done by applying stricter overlap rejection criteria. In addition, an iterative $\kappa\sigma$-clipping with $\kappa = 3$ was employed to exclude overlaps unrecognized by the automatic detection. 50 of the 623 spectra in the original data set were rejected, so that the calibration uses spectra of 573 objects (see Fig. 9; a similar plot was shown in Wisotzki et al. 2000).

A potential problem for the $B-V$ calibration is that the V band is not fully covered by the HES wavelength range. Therefore, the calibration for very red objects is inaccurate, or even impossible. As calibrators for red objects, 36 carbon stars were used, for which BV photometry was obtained at the ESO 2.2 m telescope in April 1999. Carbon stars with $B-V > 2.5$ were excluded from the fit. For $B-V \lesssim 1.0$, 778 stars from the HK survey of Beers et al. (1992), 354 FHB and other A-type stars of Wilhelm et al. (1999), and 272 objects from the northern galactic cap fields of the EC survey (Kilkenny et al. 1997) present on HES plates were used. Linear fits in three colour regions were done separately, in order to evaluate the scatter independently, and check consistency. Then, a combined fit to all 1256 unique objects was done (see Fig. 9).

The results of the fits are summarized in Table 1. Note that a single fit contains objects from a large fraction of the 329 stellar HES plates, and a wide range of object types, e.g. carbon stars, metal-poor stars, solar metallicity F- and G-type stars, field horizontal branch A-type stars, "normal" A-type stars, DAs, DBs, sdBs and quasars. The achieved accuracies are $\sigma_{U-B} = 0.092$ mag, and $\sigma_{B-V} = 0.095$ mag for the $B-V$ fit using all calibration objects together. The accuracy in $B-V$ for red ($B-V \gtrsim 1$) and blue ($B-V \lesssim 0.3$) objects is a factor of $\sim$2 worse ($\sigma = 0.15$ mag and 0.12 mag, respectively) than for intermediate $B-V$ objects ($\sigma = 0.074$ mag).

We obtain Strömgren coefficients $c_1 = (u-v)-(v-b)$ directly from HES spectra by averaging the density in the Strömgren uvb bands, and computing internal coefficients $c_{1,\mathrm{HES}}$ from that. $c_{1,\mathrm{HES}}$ was calibrated using a total of 79 stars not saturated in the HES, from three different sources. 22 metal-poor stars were taken from

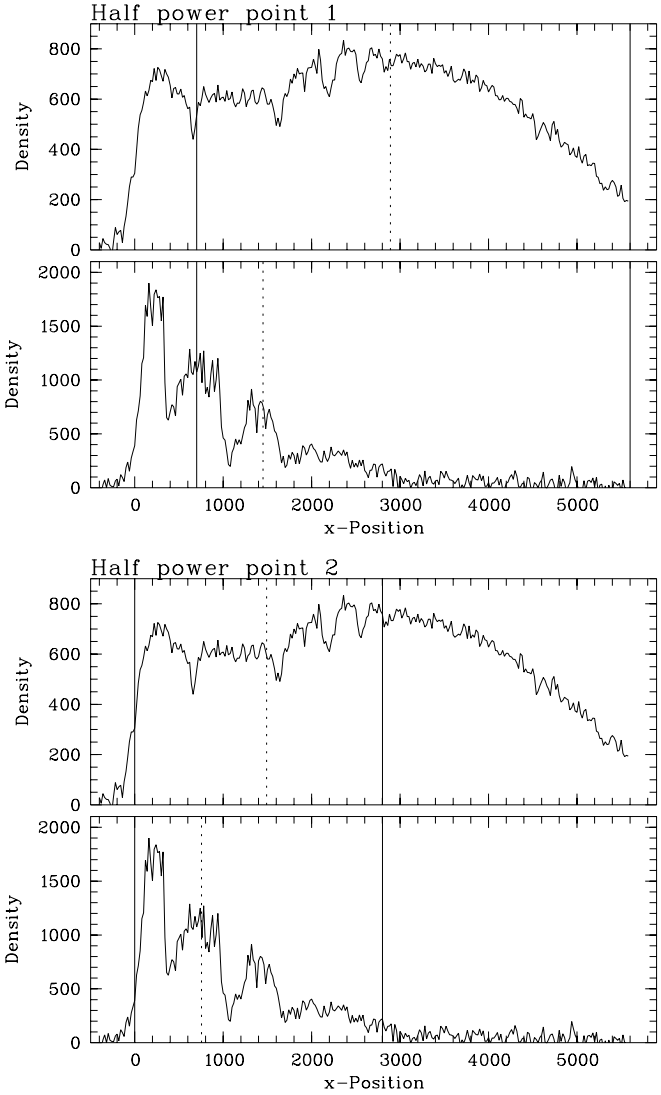

Fig. 7. Illustration of spectral half power points `x_hpp1` and `x_hpp2`. Solid lines mark the regions in which the hpps are computed; dotted lines indicate the position of the hpps

Table 1. Broad and intermediate band colour calibration fits

Colour	valid range	$N_{\rm stars}$	σ [mag]
$B-V$	$-0.6 < B-V < 2.0$	1259	0.095
$U-B$	$-1.4 < U-B < 0.8$	573	0.092
c_1	$-0.4 < c_1 < 1.0$	79	0.15

Schuster et al. (1996), 43 stars from Beers (2000, priv. comm.), of which 2 were rejected as outliers (see Fig. 10), and 16 hot subdwarfs from an updated version of the catalog of Kilkenny et al. (1988). The $1\,\sigma$ error of the calibration is 0.15 mag. c_1 can be used as a gravity indicator for early-type stars, since it measures the strength of the Balmer discontinuity.

4. Simulation of objective-prism spectra

In many stellar applications of the HES, it is not possible to generate large enough training and test samples from *real* spectra present on HES plates. This is because usually the target objects are very rare. Therefore, we have developed methods to generate *artificial* learning samples by simulations, using either model spectra, or slit spectra. In this paper we will use the simulations for the development of selection criteria. In later papers we will use sets of simulated spectra as learning samples for selection of e.g. metal-poor stars by automatic spectral classification.

The conversion of model spectra, or slit spectra, to objective-prism spectra consists of five steps:

(1) Rebinning to the non-equidistant pixel size according to the global dispersion relation for the HES;
(2) Multiplication with HES spectral sensitivity curve(s);
(3) Smoothing with a Gaussian filter, for simulation of seeing;
(4) Adding of pixel-wise, normally distributed noise;
(5) Random shift of the simulated spectrum according to the error distribution of the wavelength calibration zero point ($\pm 10\,\mu$m).

Step (4) ensures that objects of any brightness can be simulated. The $B_{\rm J}$ magnitude range corresponding to a given S/N can be read from Fig. 6.

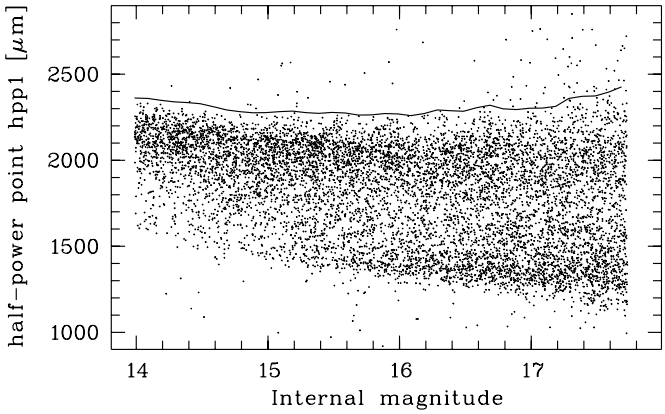

Fig. 8. Cutoff-line for bisecting point `x_hpp1` on one HES plate

4.1. HES spectral sensitivity curves

Spectral sensitivity curves (SSCs) for HES plates were determined by comparison of WD *model* spectra, rebinned to the wavelength dependent pixel size $\Delta\lambda$ of the objective-prism spectra, with objective-prism spectra of DAs on HES plates. We do not use the slit spectra directly as reference, because slit losses would produce erroneous results. The theoretical DA spectra, taken from a standard grid of WD model atmospheres (see Finley et al. 1997, for a description), were fitted to the slit spectra with methods described in Finley et al. (1997) and Homeier et al. (1998). The spectra were taken with the Boller & Chivens spectrograph attached to the ESO 1.52 m telescope, and with DFOSC at the ESO-Danish 1.54 m telescope. The atmospheric parameters of the twelve objects used in this investigation are listed in Table 2.

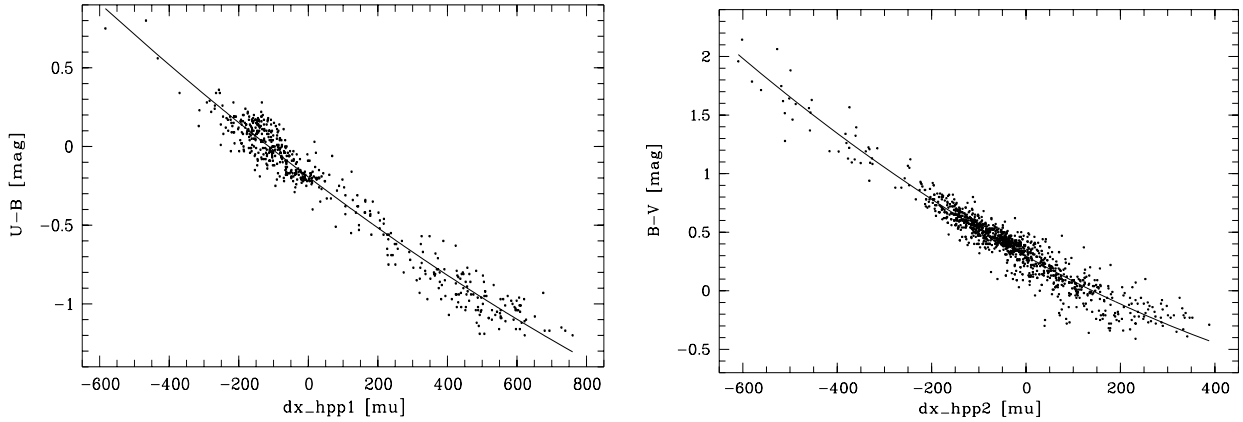

Fig. 9. Calibration of `dx_hpp1` versus $U-B$ using a sample of 573 objects from the EC and HK surveys present on HES plates (left panel); calibration of `dx_hpp2` versus $B-V$ using spectra of 1256 objects (right panel)

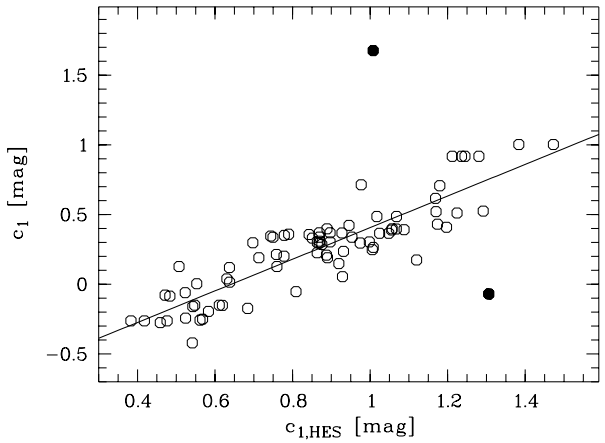

Fig. 10. Calibration of Strömgren c_1 measured in HES spectra. The two filled circles mark objects that were excluded from the fit

By comparing SSCs for plates from different plate batches, with different sky background, and generated with objects spanning a wide brightness range (see Table 3), but below the saturation threshold, we investigated the possible systematic influence of these characteristics on the shape of the SSCs. By comparing the shapes of the twelve resulting SSCs, we found that there is *no* systematic influence of object brightness, plate batch and sky background on SSC shape. The plate material of the HES is surprisingly homogenous; however, a *slight* variation of SSC shape is present, which hence must be attributed to another parameter. Since it is the blue part of the SSCs that varies, it is very likely that the time span between hypersensitization and development of the plate is responsible for the shape variations.

We grouped the twelve SSCs into four SSC classes of similar shape, and averaged them within these classes (see Fig. 11). When converting model spectra or slit spectra to objective prism spectra, we use an SSC created by averaging the four averaged SSCs with randomly assigned weights.

Table 2. Atmospheric parameters of the DA white dwarfs used for determination of spectral sensitivity curves. In the last column we give additional identifiers for objects listed in McCook & Sion (1999)

Name	$T_{\rm eff}$ [K]	$\log g$	McCook & Sion
HE 0004–5403	$18\,200 \pm 300$	8.26 ± 0.06	
HE 0059–5701	$30\,400 \pm 300$	8.08 ± 0.06	
HE 0252–3501	$17\,400 \pm 300$	7.35 ± 0.05	WD 0252–350
HE 0358–5127	$24\,100 \pm 300$	8.10 ± 0.05	
HE 0409–5154	$27\,500 \pm 300$	8.00 ± 0.06	
HE 0412–4744	$19\,300 \pm 300$	8.08 ± 0.06	
HE 0418–5326	$27\,900 \pm 200$	8.00 ± 0.05	
HE 1049–1552	$20\,200 \pm 200$	8.63 ± 0.04	WD 1049–158
HE 1058–1258	$24\,700 \pm 200$	8.84 ± 0.04	WD 1058–129
HE 1058–1334	$15\,900 \pm 300$	8.00 ± 0.07	
HE 1017–1618	$28\,600 \pm 300$	8.30 ± 0.06	WD 1017–163
HE 1017–1352	$33\,500 \pm 200$	8.25 ± 0.05	

Table 3. Averaging of spectral sensitivity curves of similar shape. `bgr` is the diffuse background (in counts) averaged over four plate quarters

#	Name	$B_{\rm J}$	Plate	`bgr`	Batch
1	HE 0004–5403	16.2	12076	1123	1D4
1	HE 1017–1618	15.8	8402	1363	1K6
1	HE 1017–1352	14.4	8402	1363	1K6
2	HE 1049–1552	14.2	9091	752	1C8
2	HE 1058–1258	14.8	9091	752	1C8
3	HE 0252–3501	16.0	11420	1039	1D4
3	HE 0358–5127	15.4	10844	765	1I3
3	HE 0409–5154	16.1	10844	765	1I3
3	HE 0412–4744	16.5	10844	765	1I3
4	HE 0059–5701	16.4	12052	1026	1D4
4	HE 1058–1334	16.6	9091	752	1C8

4.2. Adding noise

We add artificial, normally distributed noise to the converted spectra, in order to simulate objective-prism

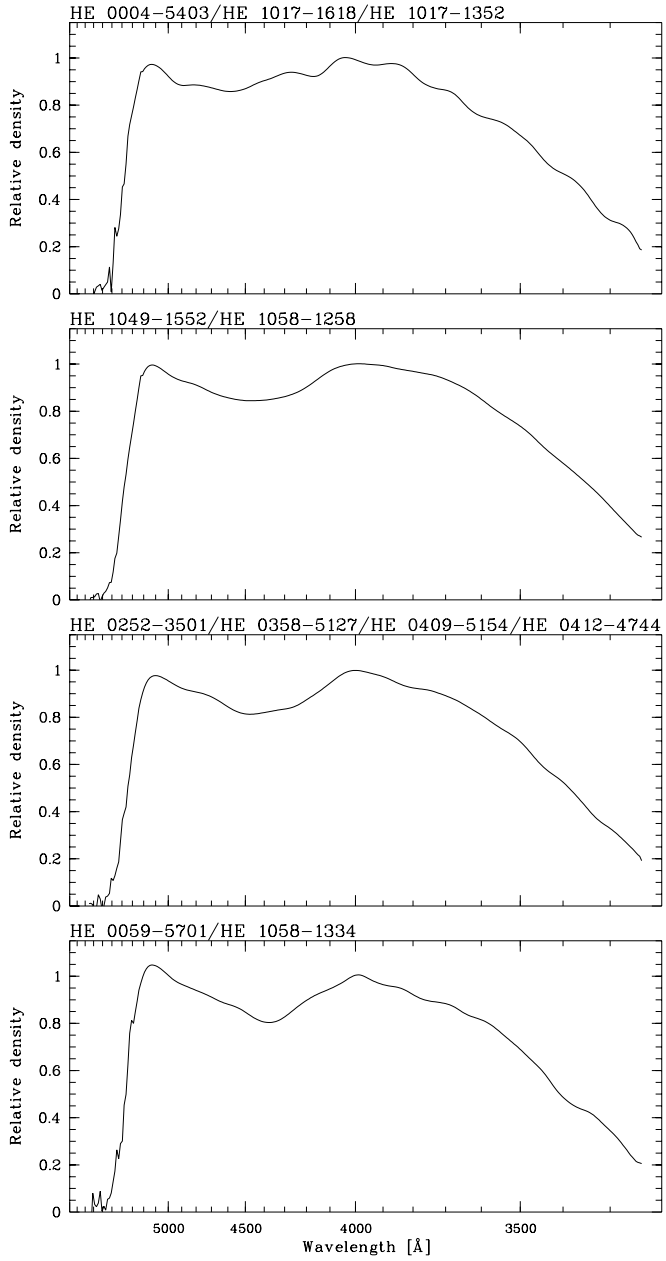

Fig. 11. Averaged spectral sensitivity curves

spectra of a desired brightness. We parameterize the S/N of a spectrum by the mean S/N in the $B_{\rm J}$ band,

$$\overline{\left(\frac{S}{N}\right)}_{B_{\rm J}} = \frac{1}{n}\sum_{i=1}^{n}\frac{D_i}{a_0 + a_1 D_i + a_2 D_i^2},$$

using the noise model described in Sect. 2.4. Since the noise depends on the density D, it is important to take care of the density variation throughout the spectrum. We thus scale the simulated spectra with a scaling factor c such that the desired mean S/N in $B_{\rm J}$ is achieved, when the appropriate amount of pixel-wise Gaussian noise is added. The mean S/N of the scaled spectrum is:

$$\overline{\left(\frac{S}{N}\right)}_{\rm new} = \frac{1}{n}\sum_{i=1}^{n}\frac{c\cdot D_i}{a_0 + a_1\cdot c\cdot D_i + a_2\cdot c^2\cdot D_i^2}. \quad (4)$$

We use one set of typical noise coefficients $a_0 \ldots a_2$ for our simulations. The appropriate scaling factor c is determined numerically from Eq. (4) using the Newton-Raphson method. A comparison of a simulated DA spectrum with a real HES spectrum is shown in Fig. 12.

5. Selection of DA white dwarfs

Since we are aiming at a very *efficient* selection of white dwarf candidates, we investigated to what extent different types of hot stars can be distinguished in the HES in a two-colour diagram ($U-B$ versus $B-V$), and in the two-dimensional feature space c_1 versus `balmsum`. We also explored several other parameter combinations, including e.g. continuum shape parameters determined by principal component analysis, but found them to be less appropriate. Using various catalogs, we identified 521 hot stars in the HES. The catalogs are: (Kilkenny et al. 1997), Wilhelm et al. (1999), an updated version of the Kilkenny et al. (1988) subdwarf catalog, and McCook & Sion (1999). Additionally, 39 HES A-type stars with known stellar parameters were included.

It turned out that high gravity stars (WDs, sdBs, and sdOs) can be distinguished quite reliably from lower gravity stars (main sequence and horizontal branch stars). However, the separation between hot subdwarfs and WDs is much more difficult, since they occupy similar regions in the parameter space (see Fig. 13). The only way to obtain clean white dwarf samples is to sacrifice completeness, as we will see below. Note however that unlike in the EC, it is possible in the HES to compile candidate samples that have *no* contamination with main sequence or horizontal branch stars.

With the spectral features automatically detected in HES spectra up to now, it is not yet possible to select DB white dwarfs; in order to do this, Helium lines would have to be added to the line list. This is currently being done.

As a first step in developing selection criteria for DAs, selection boxes in the $B-V$ versus $U-B$ and c_1 versus Balmer line sum parameter spaces were chosen such that all DAs were included (see Fig. 13). A first set of 47 HES DA candidates (hereafter referred to as the "UVES sample"; see Table A.1) selected in this way (and 72 additional WDs) were observed with VLT-UT2 and UVES between April 4 and June 6, 2000. This set includes seven re-discovered DAs listed in McCook & Sion (1999). Based on pipeline-reduced spectra, 19 of these were classified as DAs, 26 as hot subdwarfs (e.g., sdB, sdOB, sdO), two as DOs, and *none* as main sequence or horizontal branch star.

In order to decrease the contamination with hot subdwarfs, we examined if "harder" selection criteria could lead to reduced, but acceptable completeness with respect to DA white dwarfs on the one hand, and a cleaner candidate sample on the other hand. Contamination and completeness in dependence of the cutoff in Balmer line equivalent width sum was evaluated by using the subsample of those 200 stars from the learning sample of 521 stars mentioned

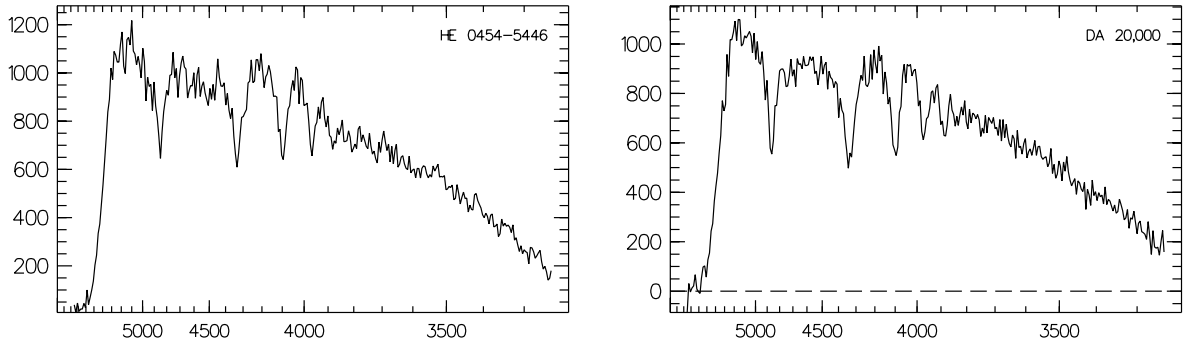

Fig. 12. HES spectrum of HE 0454–5446, a white dwarf of type DA (left panel), in comparison with a model spectrum of a DA with $T_{\rm eff} = 20\,000$ K, converted into an objective-prism spectrum and with added artificial noise (right panel). The units of the ordinates are photographic densities in arbitrary units

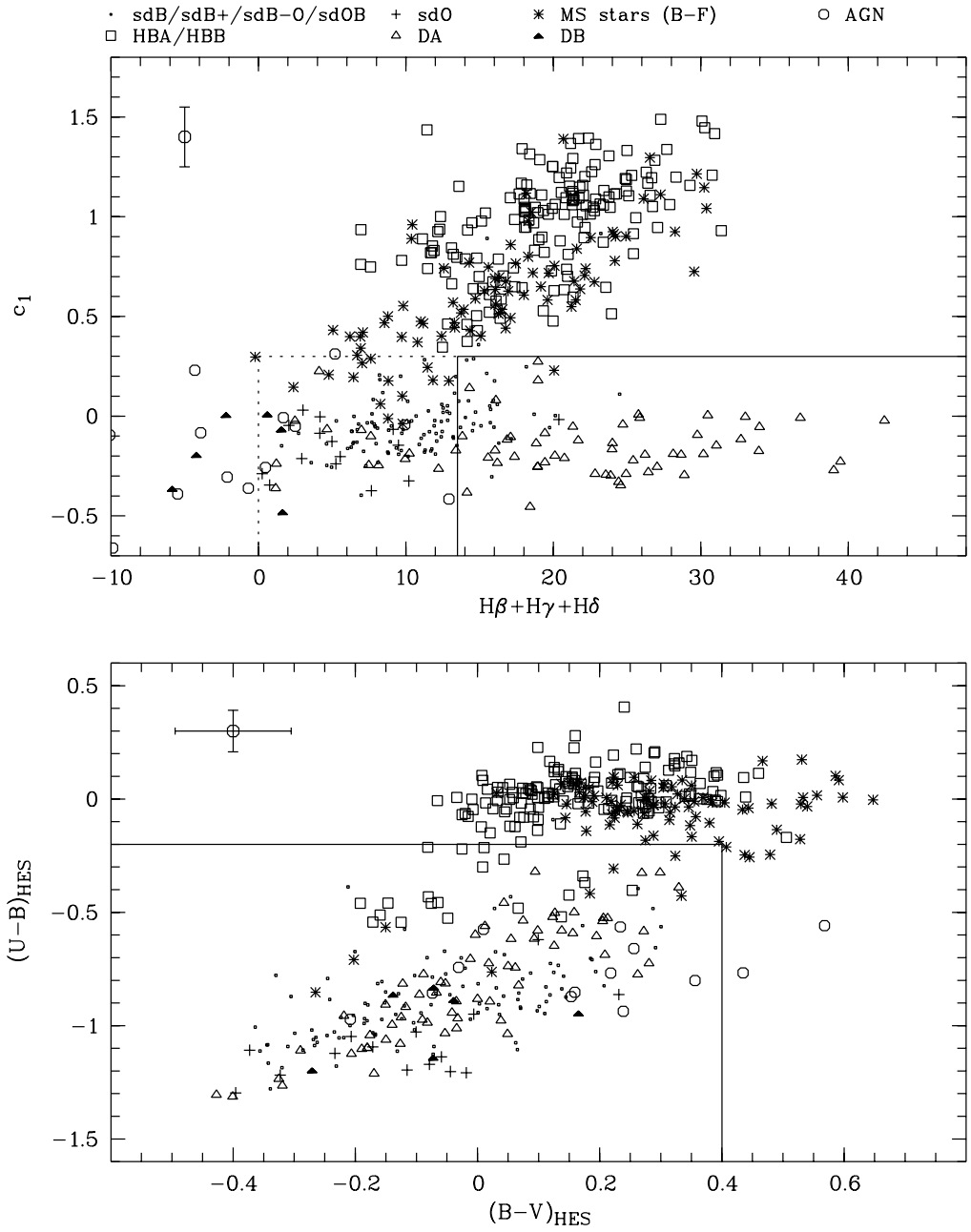

Fig. 13. DA selection in colour-colour space and c_1 versus Balmer line sum feature space. Solid lines: adopted selection box; dashed lines: additional parameter area included for the selection of the UVES sample. In the upper left corner, error bars for c_1, $U - B$ and $B - V$ are displayed

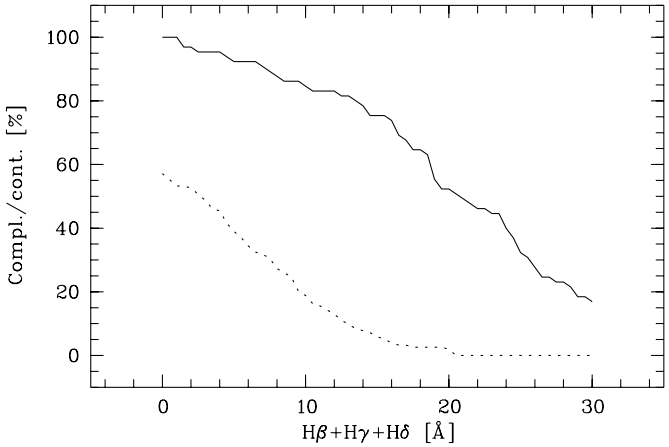

Fig. 14. Completeness (solid line) and contamination (dotted line) of the DA candidate sample as a function of Balmer line equivalent sum

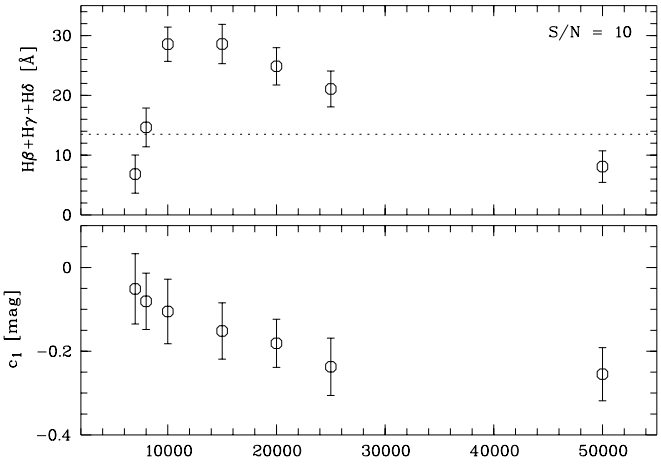

Fig. 15. Balmer line equivalent width sum and Stroemgren c_1 as a function of effective temperature, determined from simulated HES spectra with $S/N = 10$ (typically corresponding to $B_J = 16.4$). In the upper panel the `balmsum`-cutoff adopted in the HES is displayed (dotted line); the cutoff in c_1 (lower panel) is outside of the plotted parameter range. The error bars for c_1 refer to *internal* errors only

above that were located in the selection boxes also applied to the UVES sample. The relative numbers of stars were scaled such that the fraction of hot subdwarfs and WDs did reflect the fractions in the UVES sample. As can be seen from the results displayed in Fig. 14, it is possible to compile a 80% complete sample of DA white dwarfs, which is contamined by only 8% hot subdwarfs, if one confines the sample to objects with $W_\lambda(\mathrm{H}\beta + \mathrm{H}\gamma + \mathrm{H}\delta) > 13.5$ Å.

Selecting only the objects with very strong Balmer lines leads to incompleteness at the *hot* end of the DA sample (see Fig. 15), whereas DAs at $11\,000\,\mathrm{K} > T_{\rm eff} > 35\,000\,\mathrm{K}$ are very likely to be selected even at faint magnitudes (that is, at low S/N).

The final criteria,

$$\begin{aligned} W_\lambda(\mathrm{H}\beta + \mathrm{H}\gamma + \mathrm{H}\delta) &> 13.5\,\text{Å} \\ c_1 &< 0.3 \\ B-V &< 0.4 \\ U-B &< -0.2, \end{aligned}$$

were a posteriori applied to the UVES sample for an independent test. The resulting sample consists of 15 DAs; that is, the completeness is 78.9%, which is very close to what was predicted. In a sample of 15 objects, 1.2 subdwarfs are expected if the contamination is 8%, but none was found, which is consistent with the prediction.

We evaluated the *raw candidate* selection by visually inspecting a sample of 675 DA candidates at the computer screen. Visual inspection is a mandatory step in the HES in order to identify plate artifacts, the few overlaps that are not recognized by the automatic detection algorithm, and to reject mis-classified and noisy spectra. The 675 candidates were selected from the 1 789 792 overlap-free spectra with $S/N > 5$ present on 225 HES plates. We define the *specifity* of a selection as the fraction of candidate spectra ($N_{\rm can}$) drawn from the original set of spectra ($N_{\rm total}$); i.e.,

$$\text{specifity} = \frac{N_{\rm can}}{N_{\rm total}}. \qquad (5)$$

Table 4. Selection specifity and efficiency for DA white dwarfs in the HES, determined by visual inspection of candidates from 225 HES fields. For the definition of specifity see text

Specifity	1/2652
DA candidates (efficiency)	71.6%
Uncertain DA candidates	3.3%
main sequence stars (F or later)	7.4%
Subdwarf B stars	5.0%
Horizontal branch A- or B-type stars	0.9%
Quasar candidates	0.9%
Noisy spectra (no classification possible)	4.7%
Spectra disturbed by artifacts	4.1%
Overlaps	2.1%

We define the *efficiency* of a selection as the fraction of *correct* candidates among the automatically selected candidates, as judged from visual inspection of the objective-prism spectra. The results are listed in Table 4.

6. Discussion

The selection method described above allows a very efficient selection of DAs, with a high completeness (∼80%). However, this completeness estimate is based on a sample of objects that are part of the current HES data base of spectra. It is expected that a significant fraction of WDs are not part of that data base due to their proper motion (p.m.). This is because the input catalog for extraction of objective-prism spectra is generated by using the DSS I. Large proper motions and/or large epoch differences between HES and DSS I plates (13.5 years on average) currently result in a mis-extraction of spectra of objects having $\mu_\alpha \cdot \Delta t_{\text{HES-DSS I}} \gtrsim 4''$ (i.e., $\gtrsim 3$ pixels), because the spectrum of the object is looked for at the wrong place. Proper motion in direction of δ leads to an

offset of the wavelength calibration zero point, resulting in wrong equivalent width measurements (i.e., the measured widths are too low).

How large the incompleteness due to the epoch-difference problem is can roughly be estimated from a cross-identification of the HES with the catalog of McCook & Sion (1999). It lists 2 187 objects. 1 633 have an available V measurement. Of these, 1 295 (or 79.3%) lie in the HES magnitude range ($13 \lesssim V \lesssim 17.5$, assuming an average $B-V$ of zero). 606 objects are located in the southern hemisphere ($\delta < 2\overset{\circ}{.}5$), and at high galactic latitude ($|b| > 30°$). Assuming that 79.3% of these are in the HES magnitude range, we expect ∼480 WDs to be in the HES area, and detectable in the HES. Taking into account a loss of 25% due to overlapping spectra, we expect 360 known WDs to be found on all 380 HES plates, and 310 WDs on the 329 plates used so far for the exploitation of the stellar content. However, in a cross-identification procedure using a $10'' \times 10''$ search box, to compensate for the sometimes very inaccurate coordinates of McCook & Sion (1999), only 151 WDs (∼50% of the expected 310) were found.

At the chosen search box width a "saturation" of identified objects was reached; by using a larger box, no further WDs were found. However, the experience from an identification of WDs from McCook & Sion (1999) in the northern hemisphere sister project of the HES, the Hamburg Quasar Survey (HQS; Hagen et al. 1995), is that 30–40% of the objects were identified at positions more than $10''$ away from the nominal position; in many cases *much* more (up to several arc*minutes*), which explains why the identification saturation sets in already in for a $10'' \times 10''$ search box.

Furthermore, we suspect that two effects may lead to an underestimate of the completeness of the present DA selection in the HES: First, many WDs listed in McCook & Sion (1999) were discovered in the course of proper motion surveys. Therefore, the catalog is very likely to be biased towards high p.m. objects, which makes the listed WDs less likely to be detected in the HES than the real population of WDs. Second, the peak of the magnitude distribution of the WDs from McCook & Sion (1999) is more than one magnitude brighter than that of the HES, so that on average *closer* WDs (with on average higher p.m.) are listed in McCook & Sion (1999).

We conclude that the true completeness of our selection is probably higher than indicated by the simple cross-comparison. We conservatively estimate the proper motion-induced losses of DAs in the HES to be not higher than ∼20%. Special techniques to recover also high p.m. WDs are currently under development. Such techniques will permit us to construct flux-limited samples of DA white dwarfs with a very high degree of completeness, useful e.g. to determine luminosity functions.

Another problem of WD selection in the HES might currently result from the fact that in the HES stellar feature detection algorithm the width of the absorption lines is held fixed at the measured width of the instrumental profile, in order to make the algorithm more robust. However, unlike in "normal" stars, the absorption lines of WDs are so broad that they are usually resolved in the HES spectra. Therefore, the equivalent widths of their absorption lines are expected to be underestimated. Apart from more accurately measured equivalent widths, adding the line widths to the parameters to be fitted would result in the opportunity to employ a further criterion for the separation between hot subdwarfs and WDs: if the absorption lines in the spectrum of an object are significantly broader than the instrumental profile, the object is very likely to be a WD. A modification of the feature detection algorithm is in progress.

A further improvement of the selection can likely be achieved if instead of straight lines higher-order selection boundaries are used, as is the case e.g. in quadratic discriminant analysis. However, defining such selection boundaries requires *large*, and *well-defined* learning samples. A lack of model spectra for early-type stars (main sequence as well as horizontal branch stars) so far prevented us from using a learning sample of simulated objective-prism spectra for this purpose.

7. Conclusions

We described quantitative procedures for the selection of DA white dwarfs in the digital data base of the HES. Algorithms for the detection of stellar emission and absorption lines, broad- and intermediate-band colours were developed. These are not only used for the selection of DAs, but also for a couple of other interesting stars, e.g. metal-poor stars, and carbon stars. Simulation techniques allow us to convert model spectra to HES spectra, which is important for the development of selection criteria, for the compilation of learning samples used for automatic spectral classification, and for the determination of selection functions.

DAs can be selected very efficiently in the HES, as required by a currently ongoing *Large Programme* using VLT-UT2 and UVES, aiming at the detection of *double degenerates*. A first set of 440 DA candidates not listed in the catalog of McCook & Sion (1999) was identified on 225 HES plates (i.e., 59% of the survey).

We note that the UVES sample includes a double-lined DA+DA binary, and two further DAs with significant RV variations. The results will be reported elsewhere. Further investigation of these systems is in progress.

For investigations requiring *complete* samples of DAs (or other objects having high proper motions), special extraction techniques have to be employed to take into account the epoch differences between HES plates and the DSS I, since the latter is used for object detection in the HES. Such techniques are currently under development.

Acknowledgements. N. C. and D. H. acknowledge financial support from Deutsche Forschungsgemeinschaft under grants Re 353/40 and Ko 738/10-3, respectively. We thank V. Beckmann for observing a part of the DAs that were used to

determine the HES spectral sensitivity curves. Precise, photoelectric UBV and Strömgren $uvby$ photometry for HK survey stars was kindly provided by T. Beers before publication. We thank D. O'Donoghue for making EC survey photometry in digital form available to us. G. Pizarro kindly compiled a list of HES plate batches from the notes he made at the ESO Schmidt telescope. We thank the Paranal staff for carrying out the observations for the ESO Large Programme 165.H-0588 in Service Mode at VLT-UT2.

References

Beers, T. C., Preston, G. W., & Shectman, S. A. 1992, AJ, 103, 1987
Borra, E., Edwards, G., Petrucci, F., et al. 1987, PASP, 99, 535
Christlieb, N. 2000, Ph.D. Thesis, University of Hamburg, http://www.sub.uni-hamburg.de/disse/209/ncdiss.html
Demers, S., Beland, S., Kibblewhite, et al. 1986, AJ, 92, 878
Finley, D., Koester, D., & Basri, G. 1997, ApJ, 488, 375
Friedrich, S., Koester, D., Christlieb, N., et al. 2000, A&A, 363, 1040
Hagen, H.-J., Groote, D., Engels, D., et al. 1995, A&AS, 111, 195
Hewett, P., Irwin, M., Bunclark, et al. 1985, MNRAS, 213, 971
Hewett, P. C., Foltz, C. B., & Chaffee, F. H. 1995, AJ, 109, 1498
Homeier, D., Koester, D., Hagen, H.-J., et al. 1998, A&A, 338, 563
Kilkenny, D., Heber, U., & Drilling, J. S. 1988, SAAO Circ., 12, 1
Kilkenny, D., O'Donoghue, D., Koen, et al. 1997, MNRAS, 287, 867
Lamontagne, R., Demers, S., Wesemael, et al. 2000, AJ, 119, 241
Maxted, P., Marsh, T., & North, R. 2000, MNRAS, 317, L41
Maxted, P. F. L., & Marsh, T. R. 1999, MNRAS, 307, 122
McCook, G. P., & Sion, E. M. 1999, ApJS, 121, 1
Reimers, D., Jordan, S., Beckmann, V., et al. 1998, A&A, 337, L13
Reimers, D., Jordan, S., Koehler, T., et al. 1994, A&A, 285, 995
Reimers, D., Jordan, S., Koester, et al. 1996, A&A, 311, 572
Reimers, D., & Wisotzki, L. 1997, The Messenger, 88, 14
Schuster, W. J., Nissen, P. E., Parrao, L., et al. 1996, A&AS, 117, 317
Stobie, R. S., Kilkenny, D., O'Donoghue, D., et al. 1997, MNRAS, 287, 848
Wilhelm, R., Beers, T. C., & Sommer-Larsen, J. 1999, AJ, 117, 2329
Wisotzki, L., Christlieb, N., Bade, et al. 2000, A&A, 358, 77
Wisotzki, L., Köhler, T., Groote, D., et al. 1996, A&AS, 115, 227

Appendix A: The UVES sample

In Table A.1 we list coordinates, magnitudes, colours, Balmer line equivalent width sums and classifications of the UVES sample of 47 DA candidates.

Appendix B: Spectral atlas of DA and DB white dwarfs

In Fig. B.1 we display model spectra of DAs and DBs, converted to objective-prism spectra with the method described in Sect. 4. The model spectra were computed by using $\log g = 8.0$.

Table A.1. The UVES sample, with exception of the DA+DA binary, which will be published elsewhere. Coordinates are for equinox 2000.0. In the column "Type" we list object classifications based on UVES spectra

HE name	RA	Dec	B	$U-B$	$B-V$	c_1	balmsum	Type	McCook & Sion
HE 0952+0227	09 55 34.6	+02 12 48	14.7	−1.04	−0.17	−0.10	6.6	sdO	
HE 0956+0201	09 58 50.4	+01 47 23	15.6	−0.64	0.06	−0.09	24.7	DA	WD 0956+020 (DA3)
HE 0958−1151	10 00 42.6	−12 05 59	13.7	−1.05	−0.11	−0.15	2.9	DAB	
HE 1008−1757	10 10 33.4	−18 11 48	14.9	−0.91	−0.15	−0.02	2.5	DAO (sdO hot)	WD 1008−179 (DA)
HE 1012−0049	10 15 11.7	−01 04 17	15.6	−0.86	0.06	−0.07	20.5	DA	
HE 1026+0014	10 28 34.8	−00 00 29	13.9	−0.49	0.30	−0.05	23.1	DA+dM	WD 1026+002 (DA3)
HE 1033−2353	10 36 07.2	−24 08 34	16.0	−1.08	−0.34	−0.03	12.4	sdB (sdOB)	
HE 1038−2326	10 40 36.9	−23 42 39	15.9	−0.86	−0.13	0.00	10.7	sdB+cool star?	
HE 1047−0436	10 50 26.9	−04 52 36	14.7	−0.96	−0.21	−0.01	10.0	sdB	
HE 1047−0637	10 50 28.7	−06 53 26	14.3	−1.04	−0.17	−0.11	6.0	sdO	
HE 1053−0914	10 55 45.4	−09 30 58	16.4	−0.74	0.07	−0.12	30.3	DA	
HE 1059−2735	11 01 24.9	−27 51 42	15.1	−1.23	−0.35	−0.19	10.6	sdB (sdOB)	
HE 1117−0222	11 19 34.7	−02 39 05	14.3	−0.51	0.22	−0.10	24.8	DA	
HE 1130−0620	11 32 41.5	−06 36 53	15.8	−1.08	−0.09	−0.01	5.3	sdB (sdOB)	
HE 1136−2504	11 39 10.2	−25 20 55	13.8	−1.09	−0.17	−0.15	9.5	sdO	
HE 1142−2311	11 44 50.2	−23 28 18	15.4	−1.28	−0.34	−0.23	3.6	sdO	
HE 1152−1244	11 54 34.9	−13 01 17	15.8	−0.47	0.08	−0.13	28.4	DA	
HE 1200−1924	12 02 40.1	−19 41 08	14.3	−0.95	0.21	−0.26	3.0	sdO	
HE 1204−3217	12 06 47.7	−32 34 32	15.7	−0.84	−0.08	−0.21	27.5	DA	WD 1204−322 (DA)
HE 1221−2618	12 24 32.7	−26 35 16	14.7	−0.79	0.07	−0.13	6.7	sdB+cool star	
HE 1225+0038	12 28 07.8	+00 22 17	15.2	−0.45	0.34	−0.10	22.5	DA	
HE 1225−0758	12 27 47.5	−08 14 38	14.6	−0.85	0.06	−0.09	1.8	DAB, DBA?	WD 1225−079 (DZA)
HE 1229−0115	12 31 34.8	−01 32 09	13.9	−0.72	0.11	−0.08	24.6	DA	WD 1229−012 (DA4)
HE 1237−1408	12 39 56.5	−14 24 48	16.1	−1.13	−0.07	−0.19	12.0	sdOB	
HE 1238−1745	12 41 01.1	−18 01 58	14.3	−0.95	0.11	−0.16	6.1	sdO	
HE 1247−1738	12 50 22.2	−17 54 47	16.2	−0.77	0.26	−0.35	24.6	DA+dM	WD 1247−176 (DA)
HE 1256−2738	12 59 01.4	−27 54 19	16.1	−1.30	−0.31	−0.36	4.7	sdO	
HE 1257−2021	13 00 27.2	−20 37 27	16.5	−1.08	0.06	−0.12	2.8	DO/PG1159??	
HE 1258+0113	13 00 59.2	+00 57 10	16.5	−0.95	−0.01	0.00	4.2	sdO	
HE 1258+0123	13 01 10.5	+01 07 39	16.5	−0.24	0.24	0.26	31.9	DA	
HE 1309−1102	13 12 02.3	−11 18 16	16.1	−0.80	−0.17	0.03	11.4	sdB	
HE 1310−2733	13 12 50.6	−27 49 02	14.3	−1.23	−0.25	−0.28	8.2	sdO	
HE 1314+0018	13 17 24.7	+00 02 36	15.6	−1.12	0.00	−0.23	10.8	DO	
HE 1315−1105	13 17 47.4	−11 21 05	15.8	−0.42	0.23	0.05	23.3	DA	
HE 1318−2111	13 21 15.6	−21 27 18	14.6	−0.99	−0.10	−0.14	4.6	sdOB	
HE 1325−0854	13 28 23.9	−09 09 53	15.2	−0.64	0.05	0.04	27.7	DA	
HE 1333−0622	13 36 19.7	−06 37 59	16.2	−0.62	0.15	0.11	20.6	DA+dM	
HE 1349−2320	13 52 15.0	−23 34 57	15.1	−1.20	−0.04	−0.33	10.2	sdO	
HE 1352−1827	13 55 26.6	−18 42 09	16.0	−0.96	−0.17	−0.06	11.3	sdB+cool star?	
HE 1355−0622	13 57 54.3	−06 37 32	13.4	−1.12	−0.23	−0.05	2.1	sdO	
HE 1356−1613	13 59 12.5	−16 28 01	16.1	−1.21	−0.35	−0.23	7.9	sdO	
HE 1419−1205	14 22 02.1	−12 19 30	16.2	−0.98	−0.30	−0.06	11.3	sdB (sdOB)	
HE 1502−1019	15 05 22.7	−10 31 26	15.6	−1.04	−0.17	−0.25	7.3	sdOB+cool star	
HE 1511−0448	15 14 12.9	−04 59 33	15.3	−1.14	−0.32	−0.05	6.8	DA	
HE 1511−1103	15 14 17.0	−11 14 13	14.7	−1.12	−0.25	−0.11	1.7	sdO	
HE 1512−0331	15 14 50.1	−03 42 50	16.0	−1.22	−0.32	−0.35	0.8	sdO/DAO	

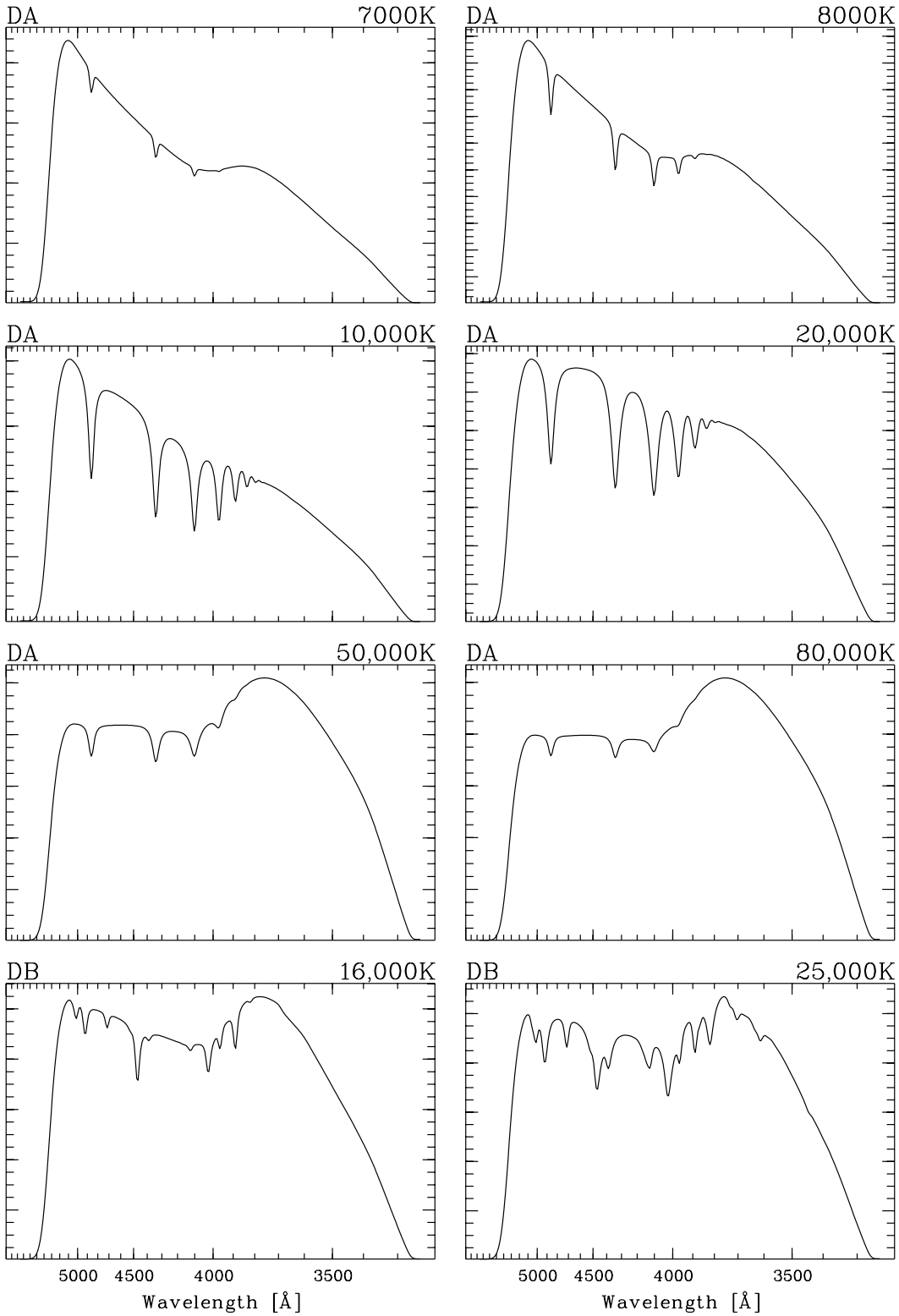

Fig. B.1. DA and DB white dwarf model spectra, converted to objective-prism spectra. Note that to these spectra no artificial noise has been added